

Physics

Electricity & Magnetism fields

Okayama University

Year 2003

Folding of the triangular lattice in a
discrete three-dimensional space:
density-matrix renormalization-group
study

Yoshihiro Nishiyama
Okayama University

This paper is posted at eScholarship@OUDIR : Okayama University Digital Information
Repository.

http://escholarship.lib.okayama-u.ac.jp/electricity_and_magnetism/176

Folding of the triangular lattice in a discrete three-dimensional space: Density-matrix renormalization-group study

Yoshihiro Nishiyama

Department of Physics, Faculty of Science, Okayama University, Okayama 700-8530, Japan

(Received 14 October 2003; published 1 July 2004)

Folding of the triangular lattice in a discrete three-dimensional space is investigated numerically. Such “discrete folding” has come about through theoretical investigation, since Bowick and co-workers introduced it as a simplified model for the crumpling of the phantom polymerized membranes. So far, it has been analyzed with the hexagon approximation of the cluster variation method (CVM). However, the possible systematic error of the approximation was not fully estimated; in fact, it has been known that the transfer-matrix calculation is limited in the tractable strip widths $L \leq 6$. Aiming to surmount this limitation, we utilized the density-matrix renormalization group. Thereby, we succeeded in treating strip widths up to $L=29$ which admit reliable extrapolations to the thermodynamic limit. Our data indicate an onset of a discontinuous crumpling transition with the latent heat substantially larger than the CVM estimate. It is even larger than the latent heat of the planar (two-dimensional) folding, as first noticed by the preceding CVM study. That is, contrary to our naive expectation, the discontinuous character of the transition is even promoted by the enlargement of the embedding-space dimensions. We also calculated the folding entropy, which appears to lie within the best analytical bound obtained previously via combinatorics arguments.

DOI: 10.1103/PhysRevE.70.016101

PACS number(s): 05.50.+q, 82.45.Mp, 05.10.-a, 46.70.Hg

I. INTRODUCTION

Statistical mechanics of membranes is regarded as a natural extension of that of polymers. The interplay between the extended geometry and the thermal fluctuations has provided even richer subjects, leading to a very active area of research [1–3]. Depending on the fine details of microscopic interactions, the behaviors of membranes are separated into a number of subgroups: In the case where the constituent molecules are diffusive, the membrane cannot support a shear, and the elasticity is governed only by the bending rigidity [4,5]. Such a membrane is called fluid (lipid) membrane, and it is always crumpled irrespective of temperatures. On the contrary, provided that fixed intermolecular connectivity is formed via polymerization, the in-plane strain is subjected to finite shear moduli. Such a membrane is called a polymerized (tethered) membrane. Contrary to the fluid membrane, the polymerized membrane is flattened macroscopically for sufficiently large rigidities, or equivalently at low temperatures [6]. (Hence, the crumpling transition separates the flat and the crumpled phases.) The flat phase is characterized by the long-range orientational order of the surface normals. It is rather exceptional that for such a two-dimensional system, continuous symmetry is broken spontaneously. To clarify this issue, a good deal of analyses have been reported so far. However, there still remain controversies whether the crumpling transition belongs to a continuous transition [7–19] or a discontinuous one accompanying appreciable latent heat [20,21].

Meanwhile, a unique alternative approach to this problem was initiated by Kantor and Jarić [22], who formulated a discretized version of the polymerized membrane. To be specific, they considered a triangular lattice (network), whose joint angle θ (relative angle between adjacent plaquettes) is taken from either $\theta=\pi$ (no fold) or $\theta=0$ (complete fold).

Because the embedding space is two-dimensional, this model is referred to as planar folding. (In the theory, we consider an unstretchable sheet without self-avoidance. Hence, the model is regarded as a discretized version of the phantom polymerized membrane with infinite strain moduli.) Owing to this discretization, the problem reduces to an Ising model; the resultant spin model is, however, subjected to a constraint which makes the problem highly nontrivial. Nevertheless, owing to the discretization, we are able to resort to numerous techniques developed in the studies of the spin models. Actually, both analytical (cluster variation) and numerical (transfer matrix) approaches have been utilized successfully [24,25]. Thereby, it turned out that the crumpling transition is discontinuous, and the discrete character of the transition is maintained even in the presence of a perturbation such as the symmetry breaking field (coupling to the spin variables).

One may be tempted to ask how this conclusion is sensitive to the enlargement of the embedding space dimensions. It is conceivable that the transition disappears altogether or that the order of the transition changes. Motivated by such an idea, Bowick and co-workers enlarged the embedding space to three dimensions [26–29]. Correspondingly, the joint angles are now taken from four distinctive values; we will explain the details afterward. However, the enlargement of the configuration space overwhelms the computer-memory space in the diagonalization procedure of the transfer matrix. The tractable strip widths L are limited within the size $L=6$, which might be rather insufficient to examine the possible systematic error of the cluster-variation approximation.

In this paper, we surmount the limitation through resorting to the density-matrix renormalization group [30–32]. This technique has proved to be successful even in the problem of soft materials such as fluid membranes [33,34]. Taking the advantage that the technique allows us to treat very large system sizes, we investigate the bulk properties of the

discrete folding in detail. Our first-principles data indicate that the crumpling transition is discontinuous, and the latent heat is considerably larger than the cluster-variation estimate. It is even larger than the latent heat of the planar folding, as first noted by the cluster-variation-method study [27]. That is, contrary to our naive expectation, the discontinuous character of the transition is even pronounced by the enlargement of the embedding-space dimensions. We will also calculate the folding entropy that has a close connection with a combinatorics problem in mathematics. Our result lies within the best analytical bound obtained via combinatorics arguments [26].

The rest of this paper is organized as follows. In the next section, we explicate the three-dimensional discrete folding. The main goal is to set up an expression for the transfer-matrix element [26]. In Sec. III, we present our scheme for the diagonalization of the transfer matrix with the density-matrix renormalization group. A preliminary simulation result for a performance check is shown as well. In Sec. IV, we perform extensive simulations. Our first-principles data are compared with the preceding cluster-variation results [27]. The last section is devoted to the summary and discussions.

II. CONSTRUCTION OF THE TRANSFER MATRIX FOR THE THREE-DIMENSIONAL DISCRETE FOLDING [26]

In this section, we set up an expression for the transfer matrix of the three-dimensional discrete folding [26]. The transfer matrix is treated numerically in the succeeding sections. To begin with, we explain how the triangular lattice (network) is embedded onto the face-centered-cubic (fcc) lattice: The fcc lattice is viewed as a packing of the three-dimensional space with octahedrons and tetrahedrons, whose vertices are shearing the lattice points of the fcc lattice; see Fig. 3 of Ref. [26]. Because faces of these polygons are all equilateral triangles, a sheet of the triangular lattice (network) can be embedded onto the fcc lattice so as to wrap these polygons in arbitrary ways. Because there are two types of polygons, the relative fold angles θ between the adjacent plaquettes (triangles) are now taken from four possibilities. That is, in addition to the cases of “no fold” ($\theta = \pi$) and “complete fold” ($\theta = 0$) that are already incorporated in the planar folding, we consider “acute fold” [$\theta = \arccos(1/3)$] and “obtuse fold” [$\theta = \arccos(-1/3)$]. [Note that we ignore the distortions of plaquettes (triangles). Hence, the limit of large strain moduli is assumed *a priori*.]

The above discretization leads to an Ising-spin representation for the membrane folding. An efficient representation, the so-called gauge rule, reads as follows [26]: We place two types of Ising variables, namely σ_i and z_i , at each triangle (rather than each joint); see Fig. 1(a). The gauge rule states that the sign change of the Ising variables with respect to neighboring triangles specifies the joint angle: That is, provided that the sign of the z_i variables changes ($z_1 z_2 = -1$), the joint angle is either acute or obtuse fold. Similarly, if $\sigma_1 \sigma_2 = -1$ holds, the relative angle is either complete or obtuse fold. Note that the above rules specify the joint angle unambiguously.

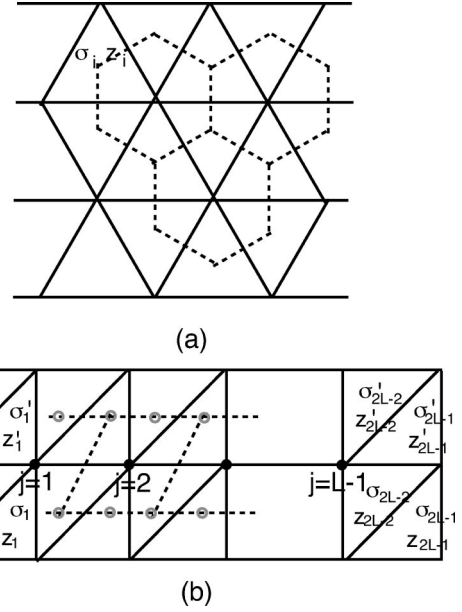


FIG. 1. (a) We consider a discrete folding of the triangular lattice embedded in the three-dimensional space. In order to specify the fold angle, we place two types of Ising variables such as z_i and σ_i at each triangle rather than at each joint (gauge rule [26]). Hence, hereafter, we consider a spin model defined on the dual (hexagonal) lattice. (b) A construction of the transfer matrix. The row-to-row statistical weight yields the transfer-matrix element. The explicit formula is given by Eq. (1). The transfer matrix is diagonalized with the density-matrix renormalization group; see Fig. 2.

Let us summarize the points: We introduced statistical variables placed at each triangle. Therefore, the resultant spin model is defined on the hexagon lattice, which is dual to the triangular lattice. Hence, the transfer-matrix strip looks like that drawn in Fig. 1(b). The row-to-row statistical weight $T_{\{\sigma_i, z_i\}, \{\sigma'_i, z'_i\}}$ yields the transfer-matrix element. However, according to Ref. [26], the Ising variables are not quite independent, and constraints should apply to the spins around each hexagon. The transfer-matrix element is given by the following form with extra factors that enforce the constraints [26]:

$$T_{\{z, \sigma\}, \{z', \sigma'\}} = \left(\prod_{j=1}^{L-1} U_j V_j \right) \exp(-H), \quad (1)$$

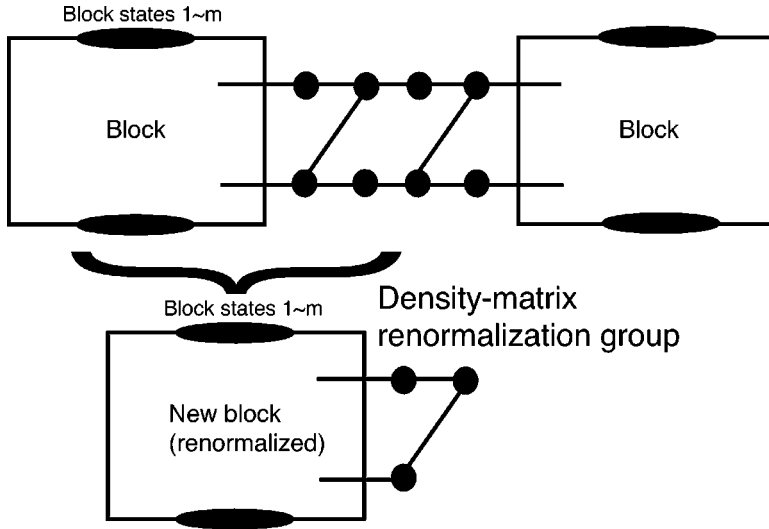
with

$$U_j = \delta(\sigma_{2j-2} + \sigma_{2j-1} + \sigma_{2j} + \sigma'_{2j-1} + \sigma'_{2j} + \sigma'_{2j+1} \bmod 3, 0), \quad (2)$$

and

$$V_j = \prod_{c=1}^2 \delta(\alpha_c(z_{2j}, z_{2j-1}, z_{2j-2}, z'_{2j-1}, z'_{2j}, z'_{2j+1}) \bmod 2, 0). \quad (3)$$

Here, $\delta(m, n)$ denotes Kronecker's symbol, and α_c is given by



$$\alpha_c(z_1, \dots, z_6) = \sum_{i=1}^6 \frac{1}{2} (1 - z_i z_{i+1}) \times \delta \left(c_0 + \sum_{j=1}^i \sigma_j - c \bmod 3, 0 \right). \quad (4)$$

[These constraints, Eqs. (2) and (3), allow 96 spin configurations around each hexagon [26]. In that sense, the resultant model is regarded as a 96-vertex model.] The Boltzmann factor $\exp(-H)$ in Eq. (1) is due to the bending-energy cost; we set the temperature T as the unit of energy; namely $T = 1$. As usual, the bending energy is given by the inner product of the surface normals of adjacent triangles. Hence, the bending energy is given by the formula

$$H = -0.5 \sum_{\langle ij \rangle} K \cos \theta = -0.5 \sum_{\langle ij \rangle} \frac{1}{3} K \sigma_i \sigma_j (1 + 2z_i z_j), \quad (5)$$

with the bending rigidity K . Here, the summation $\sum_{\langle ij \rangle}$ runs over all possible nearest-neighbor pairs i - j around each hexagon. (The overall factor 0.5 is intended to reconcile the double counting.)

The above completes the transfer-matrix construction for the discrete folding. The size of the matrix grows exponentially in the form $\propto 16^L$ with the system size L ; the definition of L is shown in Fig. 1(b). Apparently, it is an involving task to diagonalize the matrix numerically; so far, the width $L = 6$ has been achieved with the conventional full-diagonalization scheme [26,28,29]. Moreover, the open boundary condition must be imposed in order to release the constraints from the boundaries; otherwise, the constraints are too restrictive. The boundary effect deteriorates the data so that the data acquire severe finite-size corrections. In the following section, we propose an alternative diagonalization scheme which enables us to treat large system sizes.

III. NUMERICAL SIMULATION ALGORITHM: AN APPLICATION OF THE DENSITY-MATRIX RENORMALIZATION GROUP TO THE DISCRETE FOLDING

As is mentioned in the preceding section, the diagonalization of the transfer matrix (1) is cumbersome because of its

FIG. 2. Schematic drawing of the density-matrix renormalization-group (DMRG) procedure. From the drawing, we see that through one operation of DMRG, a “block” and the adjacent sites (hexagon) are renormalized altogether into a new renormalized “block.” At this time, the number of block states is retained within m ; see text. In this manner, we can diagonalize a large-scale transfer matrix through successive applications of DMRG.

overwhelming matrix size. Here, we propose an alternative approach through resorting to the density-matrix renormalization group [30–32]. The method allows us to treat large system sizes. Our algorithm is standard, and we refer the reader to the text [35] for technical details. In the following, we outline the algorithm, placing an emphasis on the changes specific to this problem. We will also present a preliminary simulation result in order to demonstrate the performance.

The basic idea of the density-matrix renormalization group is simple. It is a sort of computer-aided real-space decimation procedure with the truncation error far improved compared with the previous ones. Sequential applications of the procedure enable us to reach very long system sizes. One operation of the real-space-decimation procedure is depicted in Fig. 2. Through the decimation, the block states and the adjacent spin variables (hexagon) are renormalized altogether into new block states. The number of states for a renormalized block is kept bounded within m ; the parameter m sets the simulation precision. Such m states are chosen from the eigenstates with significant statistical weights (eigenvalues) $\{w_\alpha\}$ of a (local) density matrix [35]; this is an essential part of the density-matrix renormalization group [30], and the name comes from this.

This is a good position to address a few remarks regarding the changes specific to the present problem. First, in our simulation, in order to reduce the truncation error of the real-space decimation, we adopted the “finite-size method” [35]. We managed three sweeps at least, and confirmed that a good convergence is achieved in the sense that the error is negligible compared with the finite-size corrections. Secondly, we have applied a magnetic field H of the strength $H=2$ at an end of the transfer-matrix strip. This trick was first utilized in Ref. [29], and it aims to split off the degeneracy caused by the trivial fourfold symmetry ($\sigma = \pm 1, z = \pm 1$) of the overall membrane orientation.

We turn to a demonstration of the performance of the scheme. In Fig. 3, we present the distribution of the statistical weights $\{w_\alpha\}$ for the bending rigidity $K=0.1$, the number of states kept for a block $m=15$, and the system size $L=14$. We see that the statistical weight drops very rapidly. In fact, the 15th state exhibits very tiny statistical weight $w_{15} \approx 3$

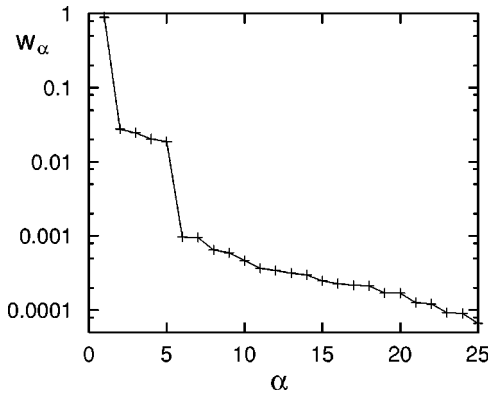


FIG. 3. Distribution of the eigenvalues (statistical weights) $\{w_\alpha\}$ (α , integer index) of the (local) density matrix [30–32] is shown. The simulation parameters are chosen from the bending rigidity $K=0.1$, the number of states kept for a block $m=15$, and the system size $L=14$. We see that w_α drops very rapidly for large α . For instance, the states up to only $\alpha=15$ cover the relevant (significant) bases with appreciable statistical weights $w_\alpha > 3 \times 10^{-4}$; the discarded weights ($\alpha > m$) indicate an amount of the truncation error. In this manner, only m selected (relevant) bases are retained for a renormalized “block” as is shown in Fig. 2.

$\times 10^{-4}$. Hence, only 15 significant bases, for instance, are sufficient to attain a precision of $\sim 3 \times 10^{-4}$; note that the statistical weight of the discarded states, namely w_α ($\alpha > m$), indicates an amount of the truncation error. In our simulation, we maintain, at most, $m=20$ bases for a renormalized block, and thus our simulation result is “exact” in a practical sense. Of course, there are finite-size corrections that are severer than the truncation error, and they are to be considered separately.

IV. NUMERICAL RESULTS

In this section, we present the numerical results. We first survey overall features for a wide range of the bending rigidity K . Guided by the findings, we perform large-scale simulations, aiming to investigate the crumpling transition and the folding entropy.

A. Preliminary survey and technical remarks

In Fig. 4, we plotted the internal energy E and the free energy F for a wide range of the bending rigidity K . Both E and F are normalized so as to represent the one-unit-cell quantities. In order to evaluate F reliably, we carried out a trick, which we explain afterward. Technical information on the simulation parameters is listed in the figure caption. From the figure, we see a clear signature of an onset of the crumpling transition at around $K_c \sim 0.2$. To be specific, we see an abrupt change of the internal energy E , and the discontinuity is pronounced as the system size L is enlarged. This tendency suggests that the singularity belongs to the first-order transition. Such a tendency was observed in the preceding full-diagonalization calculation study for $L \leq 6$ [28]. Such a discontinuous crumpling transition was predicted by the cluster-variation analysis as well [27], and we

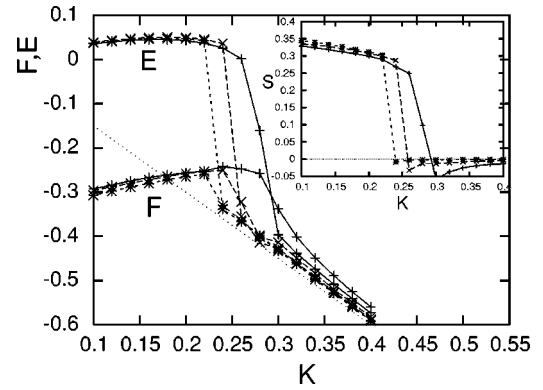


FIG. 4. We plotted the free energy F as well as the internal energy E for the bending rigidity K . The simulation parameters for each symbol are (+) $L=5$ and $m=5$, (\times) $L=6$ and $m=5$, and ($*$) $L=7$ and $m=5$. We see an abrupt change of the internal energy E , which may indicate an onset of the crumpling transition. The dotted line denotes the relation $-3K/2$ which describes the elastic energy for a completely stretched membrane. Inset: Entropy S is plotted for the bending rigidity K . In the large- K phase, the entropy appears to vanish. This result, again, indicates that the membrane is stretched completely in the flat phase.

pursue this issue further in the next subsection. In the inset, we have plotted the entropy per unit cell S . From the plot, we see that a large amount of entropy is released at the transition point. This fact shows that the membrane is flattened macroscopically in the large- K regime (flat phase). As a matter of fact, it is to be noted that the entropy vanishes in the flat phase; that is, the membrane undulations are frozen up completely withstanding the thermal disturbances. In fact, the internal energy is well fitted by the formula $E = -0.5K(3 \cos 0) = -3K/2$; see the dotted line in Fig. 4. This fact again shows that the surface normals of all plaquettes are parallel to each other ($\theta=0$). This feature is quite reminiscent of the planar folding [24]; see the Introduction. In this three-dimensional case as well, the membrane is flattened completely in the large- K phase. In the present case, however, the entropy release may be smeared out to some extent by the enlargement of the embedding space dimensions. This issue is also explored in the next subsection.

In the following, let us mention some technical remarks. First, we explain a trick to evaluate the free energy F . Although the internal energy E is calculated straightforwardly, the calculation of F requires some care. As is well known, the total strip free energy is calculated with the transfer-matrix diagonalization directly. However, because of the presence of the boundaries, the data are deteriorated by the boundary effect. (On the other hand, the presence of boundaries is vital to the numerical calculation; see Sec. II.) Moreover, through sequential applications of the normalization, the total “width” of the strip becomes obscure. In fact, the degrees of freedom processed in the early stages of normalization would be truncated out by the succeeding renormalizations. In that sense, we should place a stress upon the middle of the transfer-matrix strip, namely the middle hexagon in Fig. 2. The middle hexagon retains the full degrees of freedom (yet to be renormalized), and the boundary effect is

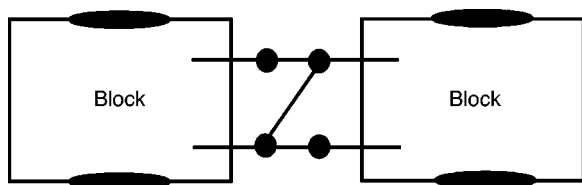


FIG. 5. From the free-energy subtraction for those transfer-matrix strips shown in the above and Fig. 2, we extracted the bulk contribution to the free energy corresponding to the middle hexagon of Fig. 2 (containing three unit cells).

less influential. In order to extract the contribution from the middle part, we managed a subtraction for those free energies with different strip widths depicted in Figs. 2 and 5. The free-energy difference yields the bulk free energy containing three unit cells. This trick is of particular importance in the succeeding subsections, where we perform numerous renormalizations.

Second, as was first noticed in Ref. [36], the density-matrix renormalization-group data exhibit a hysteresis effect. The hysteresis is due to the fact that the past information is encoded in the renormalized block. In the simulation presented in Fig. 4, we have softened the bending rigidity K gradually. In this way, we succeeded in stabilizing the flat phase. (Otherwise, one may not be able to realize the flat phase. Because the flat phase is quite peculiar in the sense that it bears zero entropy, it is very hard to reach such a state by annealing from the crumpled phase.) In the next section, we will stabilize the crumpling phase instead, because we are concerned with the crumpled state and the undulation precursor of the transition point.

B. Crumpling transition

In this subsection, we perform large-scale simulations, aiming to clarify the nature of the crumpling transition. In Fig. 6, we plotted the “excess” free energy $F+3/2K$ in the vicinity of the transition point. The technical parameters are

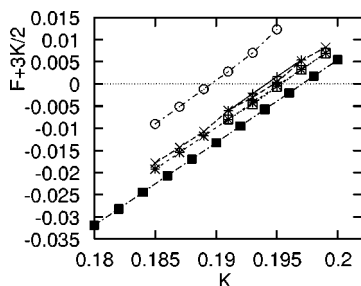


FIG. 6. “Excess” free energy $F+3K/2$ is plotted for the bending rigidity K . The simulation parameters for each symbol are (+) $L=19$ and $m=15$, (\times) $L=24$ and $m=20$, (*) $L=24$ and $m=15$, (\square) $L=29$ and $m=15$, (\blacksquare) $L=24$ and $m=5$, and (\circ) $L=14$ and $m=15$. The term $-3K/2$ comes from the known exact free energy for the flat phase. Hence, at the crumpling transition point, the excess free energy should cancel out. In this way, we obtain an estimate for the transition point as $K_c=0.195(2)$. (Because of the hysteresis effect [36], the crumpled phase is kept stabilized throughout the parameter range shown above.)

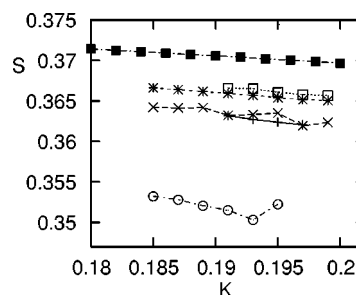


FIG. 7. Entropy S is plotted for the bending rigidity K . The entropy right at the phase transition point $K_c=0.195(2)$ yields the latent heat $Q=0.365(5)$; see text. The simulation parameters are the same as those of Fig. 6. (Because of the hysteresis effect [36], the crumpled phase is kept stabilized throughout the parameter range shown above.)

summarized in the figure caption. As is found in the preceding subsection, the excess free energy should vanish at the crumpling transition point, because the free energy in the flat phase obeys the formula $-3K/2$. In other words, in the plot, we are just comparing the free energies beside the transition point. Moreover, from the figure, we observe that the slope of the excess free energy is finite at the transition point. Hence, the crumpling transition is indeed discontinuous.

From the figure, we see that good convergence is achieved with respect to both L (system size) and m (number of retained bases for a renormalized block). In fact, the data almost overlap each other for the parameters of $m \geq 15$ and $L \geq 19$. Hence, we estimate the transition point as $K_c=0.195(2)$. Our simulation result shows that the previous cluster-variation estimate $K_c=0.18548$ is remarkably precise.

Let us mention a technical remark. As is mentioned in the above subsection, the density-matrix renormalization group exhibits a hysteresis effect. Hence, upon increasing the bending rigidity gradually, we are able to retain the crumpling phase. Taking advantage of those features rather specific to this particular problem and the methodology, we are able to determine the crumpling transition very precisely in terms of the excess free energy.

As mentioned above, our data depicted in Fig. 6 suggest that the crumpling transition is discontinuous. In order to estimate the amount of the latent heat, in Fig. 7 we plotted the entropy S in close vicinity of the transition point. (The technical parameters are the same as those of Fig. 6.) Note that the entropy at the transition point yields the latent heat, because whole entropy is released at the crumpling transition. (Again, owing to the hysteresis effect, the crumpling phase is kept stabilized throughout the parameter range shown in the figure.) In this way, we estimate the latent heat as $Q=T\Delta S=0.365(5)$.

Our first-principles estimate of the latent heat may be intriguing. First, the present estimate appears to be substantially larger than that of the cluster-variation study $Q_{CV,3d}=0.229(=0.18548 \times 1.237)$ [27]. [Here, the contribution 1.237 comes from a “jump in the energy-like correlation function” [27]. Hence, multiplying it by the bending-rigidity modulus $K_c=0.18548$, we obtain the latent heat; see the for-

mula for the bending energy (5).] As a matter of fact, our data of Fig. 7 indicate that the entropy is kept almost unchanged even in the vicinity of the transition point. This fact tells us that the phase transition occurs abruptly without any precursor. [Almost all “folding entropy” $S(K=0)$, which is calculated in the next subsection, is released at the transition point actually.] We think that the constraints, Eqs. (2) and (3), give rise to such a notable suppression of the undulation precursory of the crumpling transition. In this sense, it is suspected that the constraints are not fully appreciated by the single-hexagon-cluster approximation in the preceding work. Second, nevertheless, it is still counterintuitive that the latent heat is even larger than that of the planar folding $Q_{CV,2d}=0.11(=0.1013 \times 1.047)$ obtained by the cluster-variation method [25,27]. Naively, one would expect that the latent-heat release is smeared out by the enlargement of the embedding spatial dimensions. Contrary to such a naive expectation, our data indicate that the discontinuous nature of the transition is enhanced by the enlargement of the embedding spatial dimensions. The tendency observed in our simulation data supports the claim that the crumpling transition is discontinuous [20,21].

C. Folding entropy

In this subsection, we calculate the folding entropy, namely the entropy in the absence of the bending rigidity ($K=0$). This quantity has a close connection with mathematics; in the absence of the elastic term, the thermodynamics reduces to a pure entropic problem regarding the assessment of the volume in the configuration space. Hence, a combinatorics argument applies. As a matter of fact, in the case of the planar folding, the folding entropy S_{2d} is obtained exactly in the context of the coloring problem [23,37,38], namely $S_{2d} = \ln q_{2d}$ with $q_{2d} = \sqrt{3} \pi \Gamma(1/3)^{3/2} / 2 = 1.20872$. As for the three-dimensional discrete folding, an exact bound $1.436 \leq q_{3d} \leq 1.589$ has been known [26], namely $0.361 \leq S \leq 0.463$. [We see that the effective degrees of freedom per unit cell are reduced considerably owing to the constraints (2) and (3).] Both cluster variation $q=1.42805$ [27,29] and numerical estimates $q=1.43(1)$ [26] lie slightly out of the analytic bound. It may be thus desirable to make an assessment of the folding entropy with the present first-principles simulation scheme.

In Fig. 8, we plotted the entropy S at $K=0$ against $1/L^2$. The simulation parameters are summarized in the figure caption. From the figure, we see that a good convergence is achieved with respect to both L and m . Thereby, we estimate the folding entropy in the thermodynamics limit as $S=0.378(2)$. Our estimate lies within the aforementioned analytic bound actually. Remarkably enough, it is close to the lower bound (4% error), suggesting that the argument [26] setting the lower bound is indeed capturing the essential mechanism for the folding entropy.

V. SUMMARY AND DISCUSSIONS

We have investigated the three-dimensional discrete folding by means of the density-matrix renormalization group.

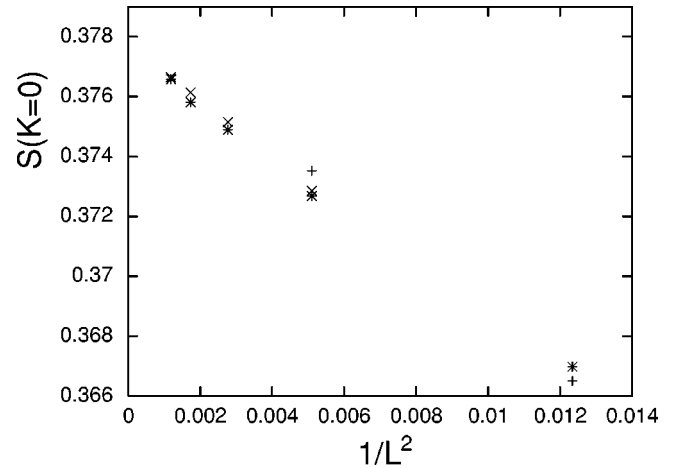


FIG. 8. Folding entropy $S(K=0)$ is plotted for $1/L^2$. The simulation parameter for each symbol is (+) $m=10$, (\times) $m=15$, and ($*$) $m=20$. Taking an extrapolation to the thermodynamic limit $L \rightarrow \infty$, we obtain an estimate $S=0.378(2)$. Our estimate lies within the best analytic bound [26]; see text.

The method allows us to treat large system sizes. In fact, we succeeded in diagonalizing the transfer matrix with the strip widths up to $L=29$. The system sizes treated in the present study are far improved, compared to the past limitation of $L=6$. Taking the advantage, we could take reliable extrapolations to the thermodynamic limit; see Fig. 8, for instance. Moreover, from the figure, we confirm that the (renormalization-group) truncation error is fairly negligible, $\sim 10^{-4}$. Actually, the truncation error is far smaller than the finite-size corrections, and it is controlled systematically by the parameter m ; see Fig. 3 as well.

Encouraged by these achievements, we turned to the analyses of the crumpling transition and the folding entropy. Here, we also aimed to examine the preceding analytical treatment [29] based on the cluster-variation approximation; the approximation has been known to be reliable in the case of the planar folding [25], whereas it remained unclear whether it is validated for the three-dimensional folding. Performing large-scale simulations, we estimated the crumpling transition point $K_c=0.195(2)$ and the latent heat $Q=0.365(5)$; see Figs. 6 and 7. Concerning K_c , the numerical result is in good agreement with the cluster-variation estimate $K_c=0.18548$. As for the latent heat, however, our simulation result appears to be substantially larger than the prediction by the cluster-variation method $Q_{CV,3d}=0.229$. Our first-principles data suggest that the constraints, Eqs. (2) and (3), were not fully appreciated by the (single-hexagon cluster) approximation in the preceding study. Namely, in reality, the undulation precursory of the crumpling transition is suppressed considerably by the constraints. As a matter of fact, the latent heat in the three-dimensional folding is even larger than that of the planar folding, as first noted by the cluster-variation study [27]. This fact might be quite counterintuitive, because one expects that the entropy release should be smeared out by the embedding-space enlargement. Our first-principles simulation shows that such a naive expectation does not hold, and in reality, the discontinuous nature of the crumpling transition is even promoted by the embedding-

space enlargement. [Actually, almost all folding entropy $S(K=0)$ is released abruptly at the transition point.] In this sense, the tendency observed in our simulation data supports the claim that the crumpling transition is discontinuous [20,21].

Let us turn to addressing the entropy in the absence of the bending rigidity $K=0$. This quantity is often referred to as the folding entropy, and it has a close connection with a combinatorics problem in mathematics [23,37,38]; note that because of $K=0$, the thermodynamics is governed solely by the entropy (configuration-space volume). In Ref. [26], an analytic bound $0.361 \leq S \leq 0.463$ was derived via ingenious combinatorics arguments. The preceding results [27,29] are, however, slightly out of this bound. We performed extensive simulation for the folding entropy with the elastic constant switched off; see Fig. 8. Thereby, we estimated the folding entropy as $S=0.378(2)$. It lies within the best analytic bound, and actually, it is almost overlapping the lower bound (4%

error). Hence, it is suggested that the analytical argument leading to this lower bound is capturing the essence of the folding mechanism.

Our first-principles simulation reveals that the discontinuous character of the transition is promoted by the enlargement of the embedding-space dimensions. Possibly, the constraints, Eqs. (2) and (3), give rise to such a notable discontinuity. Hence, it would be of considerable interest to release the constraint somehow, and see how the nature of the transition changes. The constraint release, however, results in a severe increase of the nonzero elements of the transfer matrix, and is thus computationally demanding. This problem will be addressed in future study.

ACKNOWLEDGMENTS

This work is supported by a Grant-in-Aid for Young Scientists (No. 15740238) from Monbusho, Japan.

-
- [1] D. Nelson, T. Piran, and S. Weinberg, *Statistical Mechanics of Membranes and Surfaces, Vol. 5 of The Jerusalem Winter School for Theoretical Physics* (World Scientific, Singapore, 1989).
- [2] P. Ginsparg, F. David, and J. Zinn-Justin, *Fluctuating Geometries in Statistical Mechanics and Field Theory* (Elsevier Science, The Netherlands, 1996).
- [3] M. J. Bowick and A. Travesset, *Phys. Rep.* **344**, 255 (2001).
- [4] P. Canham, *J. Theor. Biol.* **26**, 61 (1970).
- [5] W. Helfrich, *Z. Naturforsch. C* **28**, 693 (1973).
- [6] D. R. Nelson and L. Peliti, *J. Phys. (France)* **48**, 1085 (1987).
- [7] Y. Kantor, M. Kardar, and D. R. Nelson, *Phys. Rev. Lett.* **57**, 791 (1986).
- [8] Y. Kantor, M. Kardar, and D. R. Nelson, *Phys. Rev. A* **35**, 3056 (1987).
- [9] M. Baig, D. Espriu, and J. Wheeler, *Nucl. Phys. B* **314**, 587 (1989).
- [10] J. Ambjørn, B. Durhuus, and T. Jonsson, *Nucl. Phys. B* **316**, 526 (1989).
- [11] R. Renken and J. Kogut, *Nucl. Phys. B* **342**, 753 (1990).
- [12] R. Harnish and J. Wheeler, *Nucl. Phys. B* **350**, 861 (1991).
- [13] M. Baig, D. Espriu, and A. Travesset, *Nucl. Phys. B* **426**, 575 (1994).
- [14] M. Bowick, S. Catterall, M. Falcioni, G. Thorleifsson, and K. Anagnostopoulos, *J. Phys. I* **6**, 1321 (1996).
- [15] J. F. Wheeler and P. Stephenson, *Phys. Lett. B* **302**, 447 (1993).
- [16] J. F. Wheeler, *Nucl. Phys. B* **458**, 671 (1996).
- [17] F. David and E. Guitter, *Europhys. Lett.* **5**, 709 (1988).
- [18] P. Le Doussal and L. Radzihovsky, *Phys. Rev. Lett.* **69**, 1209 (1992).
- [19] D. Espriu and A. Travesset, *Nucl. Phys. B* **468**, 514 (1996).
- [20] M. Paczuski, M. Kardar, and D. R. Nelson, *Phys. Rev. Lett.* **60**, 2638 (1988).
- [21] J.-Ph. Kownacki and H. T. Diep, *Phys. Rev. E* **66**, 066105 (2002).
- [22] Y. Kantor and M. V. Jarić, *Europhys. Lett.* **11**, 157 (1990).
- [23] P. Di Francesco and E. Guitter, *Europhys. Lett.* **26**, 455 (1994).
- [24] P. Di Francesco and E. Guitter, *Phys. Rev. E* **50**, 4418 (1994).
- [25] E. N. M. Cirillo, G. Gonnella, and A. Pelizzola, *Phys. Rev. E* **53**, 1479 (1996).
- [26] M. Bowick, P. Di Francesco, O. Golinelli, and E. Guitter, *Nucl. Phys. B* **450**, 463 (1995).
- [27] E. Cirillo, G. Gonnella, and A. Pelizzola, *Phys. Rev. E* **53**, 3253 (1996).
- [28] M. Bowick, P. Di Francesco, O. Golinelli, and E. Guitter, *Proceedings of the 4th Chia Meeting on Condensed Matter and High Energy Physics* (World Scientific, Singapore 1995).
- [29] M. Bowick, O. Golinelli, E. Guitter, and S. Mori, *Nucl. Phys. B* **495**, 583 (1997).
- [30] S. R. White, *Phys. Rev. Lett.* **69**, 2863 (1992).
- [31] S. R. White, *Phys. Rev. B* **48**, 10345 (1993).
- [32] T. Nishino, *J. Phys. Soc. Jpn.* **64**, 3598 (1995).
- [33] Y. Nishiyama, *Phys. Rev. E* **66**, 061907 (2002).
- [34] Y. Nishiyama, *Phys. Rev. E* **68**, 031901 (2003).
- [35] I. Peschel, X. Wang, M. Kaulke, and K. Hallberg, *Density-Matrix Renormalization: A New Numerical Method in Physics* (Springer-Verlag, Berlin, 1999).
- [36] A. Gendiar, and T. Nishino, *Phys. Rev. E* **65**, 046702 (2002).
- [37] R. J. Baxter, *J. Math. Phys.* **11**, 784 (1970).
- [38] R. J. Baxter, *J. Phys. A* **19**, 2821 (1986).